



A Lunar Surface Mission to Trace Plasma Histories Through Solar Wind-Derived Water in the Regolith

Funmilayo Adeeye

Department of Aeronautics and Astronautics, Stanford University

1 Introduction

This project proposes a lunar surface mission to investigate the origin and nature of solar wind-derived water in the Moon's regolith, particularly in the middle latitudes where recent studies have revealed high abundances of solar wind-implanted water [1]. A rover equipped with in-situ sensing instruments will analyze the isotopic and molecular composition of water in the regolith. By doing so, the mission aims to backtrack and characterize the properties of solar wind plasmas that formed these hydroxyl and water molecules.

This study bridges surface exploration and heliophysics, using the Moon's surface as a long-term record of solar wind interactions. It holds implications for understanding lunar resource potential (ISRU), the evolution of space weathering, and the plasma environment in the Earth-Moon system [2].

1.1 Background

Historically, the Moon was considered arid. However, in 2009, NASA's LCROSS mission detected water ice in permanently shadowed craters at the lunar south pole. Subsequent missions, such as India's Chandrayaan-1, confirmed the presence of hydroxyl (OH) and water molecules on the lunar surface. These discoveries have profound implications for future lunar exploration and potential colonization[3, 4].

Water (H_2O) on the lunar surface is of significant interest owing to its crucial role in human survival. Infrared reflectance spectra from missions such as *Cassini*, *Deep Impact*, and *Chandrayaan-1* have revealed the widespread presence of H_2O , predominantly in the form of hydroxyl (OH). Recent laboratory studies also show that massive water production can occur from lunar ilmenite through reaction with endogenous hydrogen in the regolith, further supporting the potential for in-situ resource utilization (ISRU) on the Moon [2].

Several theories have been proposed to explain the presence of water on the Moon. High-energy impacts from comets, asteroids, and meteoroids have long been considered a potential source. When such objects strike the Moon's surface, they generate extreme thermal and shock conditions that ionize the lunar regolith. This process produces reactive species such as O^+ and H^+ ions, which can recombine into volatile compounds like water (H_2O). Over billions of years, these cumulative impacts may have contributed to both the delivery and synthesis of water within the lunar soil and subsurface [1, 5].

Another leading theory involves solar wind implantation. Hydrogen ions (protons) from the solar wind continuously bombard the lunar surface, especially in sunlit regions. When these protons interact with oxygen atoms embedded in lunar minerals such as olivine, plagioclase, and pyroxene, hydroxyl (OH) and water (H_2O) molecules can form. Recent spectral and microstructural analysis of regolith collected during the Chang'E-5 mission confirmed the presence of solar wind-derived water. These findings reveal that the

formation of OH/H₂O is influenced by exposure time, mineral composition, and crystallographic structure. Moreover, by comparing in-situ sample measurements with remote sensing observations, researchers have estimated surface water distributions across the Moon’s middle latitudes [6].

Water on the Moon—particularly that formed by solar wind interactions—challenges our understanding of planetary surfaces and volatile dynamics in airless bodies. While missions like Chandrayaan-1 and LCROSS have confirmed the presence of water and OH [3, 4], key questions remain about how these molecules are formed, how they vary across locations and depths, and what they reveal about the plasmas that created them.

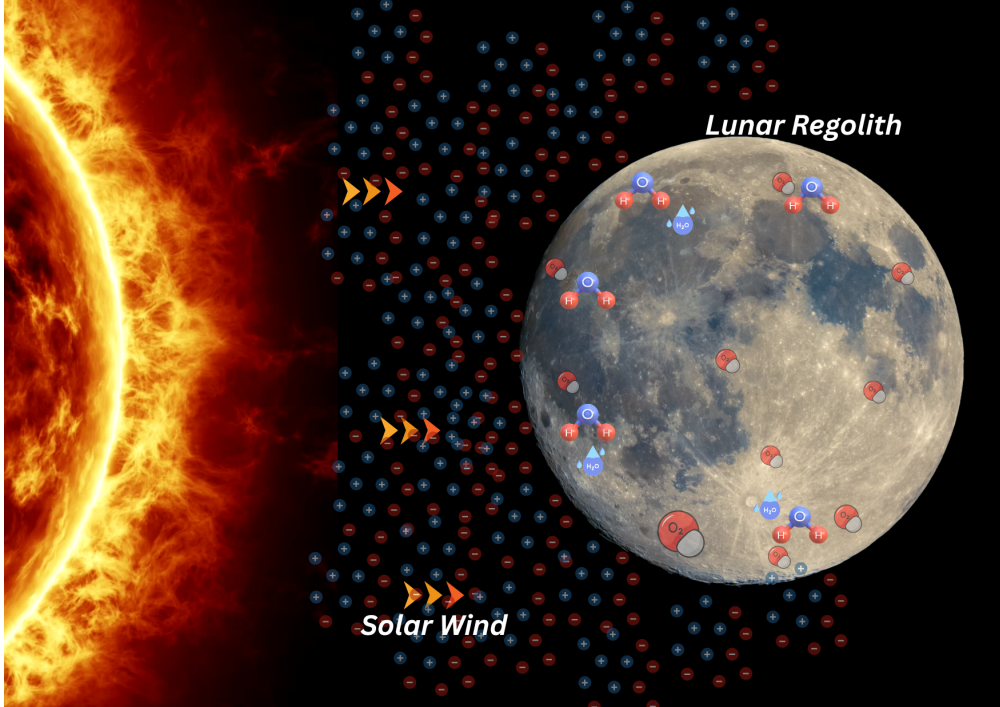


Figure 1: Conceptual image of solar wind hydrogen ions interacting with oxygen in lunar minerals to form hydroxyl and water molecules. This process primarily occurs in sunlit regions of the Moon.

Surface water content has been found to exhibit diurnal variations, suggesting a dynamic equilibrium between continuous solar wind hydrogen implantation and thermally driven loss mechanisms. These variations are interpreted as evidence for an active, rather than static, hydration process on the Moon’s surface. Lunar soil analyses and laboratory ion irradiation experiments support the hypothesis that solar wind hydrogen acts as an exogenous source. Specifically, solar wind protons are implanted into the outermost layers of mineral grains—such as olivine, plagioclase, and pyroxene—forming hydroxyl (OH) bonds and, in some conditions, molecular water (H₂O). Recent studies also propose Earth wind (magnetotail plasma) as an additional, intermittent contributor to lunar surface hydration during the Moon’s passage through Earth’s magnetosphere [7].

Laboratory simulations have successfully replicated the process of solar wind-induced water formation. NASA-led experiments demonstrated that when solar wind protons are directed at lunar soil analogs, hydroxyl (OH) and water (H₂O) molecules can form on the surfaces of silicate minerals under vacuum and temperature conditions akin to the lunar environment [8, 9]. These findings validate the theory that solar wind is a primary contributor to surface hydration on airless bodies.

Complementing these experiments, remote sensing instruments such as the Moon Mineralogy Mapper (M³) aboard India’s Chandrayaan-1 mission have provided robust spectral evidence for the presence of hydroxyl and water across vast regions of the lunar surface, particularly in the mid- and high-latitude regions [3]. Notably, the Chang’E-5 samples have revealed high concentrations of solar wind-derived water in the middle latitudes, reinforcing the idea that these regions serve as critical zones for understanding the

interaction between solar wind and lunar regolith [6]. Taken together, these findings underscore the scientific value of exploring mid-latitude sites to directly investigate the abundance, origin, and variability of solar wind-derived water on the Moon.

Recent findings, particularly from the *Chang'e-5* lunar mission, have identified the Moon's middle latitudes (approximately 20°–60° in both hemispheres) as key regions for studying solar wind-derived water. These areas exhibit higher hydroxyl (OH) and water (H_2O) concentrations due to consistent solar wind exposure without the extreme thermal variations experienced at the equator or the polar extremes. Minerals such as olivine, pyroxene, and plagioclase in the lunar regolith serve as host matrices for this hydration, driven primarily by proton implantation from the solar wind [6].

The middle latitudes also facilitate the study of diurnal hydration cycles, where water content fluctuates with solar illumination and surface temperature. These variations imply a dynamic equilibrium between solar wind implantation and thermal desorption processes [10]. Furthermore, laboratory simulations and ion irradiation experiments support the interpretation that hydrogen from the solar wind is the dominant exogenous source of surficial lunar water.

Consequently, targeting these regions for future in situ exploration or sample-return missions can significantly advance our understanding of solar wind–regolith interactions and water formation on airless planetary bodies.

The *solar wind implantation hypothesis* is a very intuitive and promising model, especially in sunlit and mid-latitude regions. But to understand the history and variability of the solar wind itself (and potentially other plasma types), we must link water molecule signatures (e.g., isotopic ratios, binding states) with space weather conditions over time. This mission is motivated by the opportunity to use regolith chemistry to characterize ancient solar wind properties, determine variability in water formation mechanisms based on location, regolith composition, and solar exposure ,and build a bridge between planetary surface science and heliophysics.

1.2 Mission Goals

The overarching goal of this mission is to investigate the chemical and isotopic signatures of solar wind-derived water in the Moon's mid-latitude regolith in order to reconstruct the history and variability of the lunar plasma environment. Specifically, the mission will deploy a mobile rover equipped with a suite of in-situ analytical instruments to the *Oceanus Procellarum* region (approximately 43°N latitude), near the landing site of the *Chang'e-5* mission. This area, classified as a mid-latitude site, offers a unique opportunity to study the influence of solar wind interactions under moderate insolation conditions.

Recent findings from the *Chang'e-5* mission have shown a high abundance of solar wind-derived water in mid-latitude lunar soils, confirming that these regions—often overlooked compared to the polar and equatorial zones—serve as significant reservoirs of water formed via proton implantation processes [11].The rover's mission will involve collecting and analyzing regolith samples at multiple depths and locations to map the molecular and isotopic structure of hydroxyl (OH) and water (H_2O) within the soil. These measurements will provide insights into temporal variations in solar wind composition, implantation efficiency, and retention mechanisms.

Solar wind is considered the dominant source of surface hydroxyl in sunlit, non-polar lunar regions. However, the precise mechanisms governing its interaction with the regolith remain under active investigation. By assessing isotopic ratios such as D/H and comparing them with modeled solar wind compositions, the mission aims to reverse-engineer plasma characteristics from the water signatures preserved in the regolith. This builds on the hypothesis that lunar surface hydration patterns can be used as long-term records of heliospheric variability and space weather history [2].

This mission will compare regolith samples across terrain features, such as mare vs. highland soils, slope vs. flat surfaces, and sun-exposed vs. shadowed regions. By tracking how hydroxyl and water concentrations change with local topography, surface temperature, and solar exposure, the mission will help refine existing models of diurnal hydration cycles and implantation-retention-release dynamics. The Moon Mineralogy Mapper (M3) aboard *Chandrayaan-1* provided global spectral data on OH/ H_2O signatures, showing widespread hydration across the Moon, especially at high latitudes and near sunrise/sunset terminators [3].

This mission will localize and validate those remote-sensing results using ground-truth measurements, contributing to a better understanding of how surface hydration changes over time and space.

Understanding the distribution and chemistry of water is key to evaluating its extractability and usefulness for future lunar missions. The rover will assess how tightly bound water molecules are to regolith grains, which affects how much energy is required to release them. Regions with weakly bound or surface-adsorbed OH are more accessible and therefore more promising for in-situ resource utilization (ISRU). This effort aligns with broader goals under NASA’s Artemis program and China’s Lunar South Pole missions to establish sustainable human presence on the Moon [4].

One of the most novel and interdisciplinary goals of this mission is to use the Moon as a “solar wind integrator,” capturing and preserving the chemical signatures of solar plasma over time. This approach offers a new way to study heliophysics from a planetary geology perspective. While satellites like SOHO and ACE provide real-time solar wind data, they don’t offer the long-term geological context that regolith-embedded water molecules do. This strategy supports a paradigm shift in how we study planetary weathering, solar-terrestrial relationships, and exoplanet habitability by examining how water forms and evolves under plasma bombardment on airless bodies.

2 Orbital Requirements

This mission is focused on studying solar wind-derived water and plasma-related phenomena at mid-latitude regions of the Moon—specifically around the *Oceanus Procellarum* area. An orbit or descent path that allows direct access to *Oceanus Procellarum* (approximately 43°N) is crucial. The orbital plan should also support post-landing rover operations and sampling, possibly using a low-altitude parking orbit before descent. Since the rover is meant to land in the mid-latitude region (approximately 20°–60° North or South), the orbital inclination must allow it to pass over that region regularly.

2.1 Destination and Duration

This mission proposes to explore the Oceanus Procellarum region on the Moon, with specific focus on the mid-latitude zone around $\sim 43^{\circ}\text{N}$. The selection of this site is driven by both scientific significance and the heritage of mission success, particularly demonstrated by China’s Chang’e 5 mission, which landed at 43.06°N , 51.92°W and successfully returned ~ 1.7 kg of lunar samples to Earth in December 2020 [12, 13]. The region is part of a geologically young mare basalt plain and offers a unique opportunity to investigate solar wind-derived water, plasma interactions, and space weathering processes on the Moon’s surface.

Oceanus Procellarum is particularly compelling due to its moderate titanium concentrations, high thorium levels, and exposure to solar wind, which plays a significant role in hydrogen implantation—a precursor to hydroxyl (OH^-) and water (H_2O) formation on lunar soil [11]. The mid-latitude location also provides a balanced environment between the harsh radiation and temperature variations of the lunar equator and the colder, permanently shadowed regions near the poles. Inspired by Chang’e 5’s 23-day timeline, this mission proposes a total duration of 25–30 days from launch to sample return. This includes 3–5 days of surface operations, allowing the rover or lander to perform in-situ analysis and sampling, 10–15 days of orbital support, including remote sensing and communications relay, Remaining time allocated for transit to and from the Moon and rendezvous/docking operations in lunar orbit.

The decision for a ~ 5 -day surface operation is based on thermal cycle management and lunar day duration (~ 14 Earth days), ensuring activities occur during favorable illumination periods.

2.1.1 Orbital Parameters and Access Justification

The mission architecture includes a **low lunar orbit (LLO)** of approximately 200 km with an orbital inclination of $\sim 43^{\circ}$, which allows consistent overpasses of the landing site for potential descent and rendezvous operations. The ground track coverage of a spacecraft in LLO is directly related to its inclination and nodal regression.

To estimate the orbital period, we use:

$$T = 2\pi \sqrt{\frac{r^3}{GM}}$$

Where:

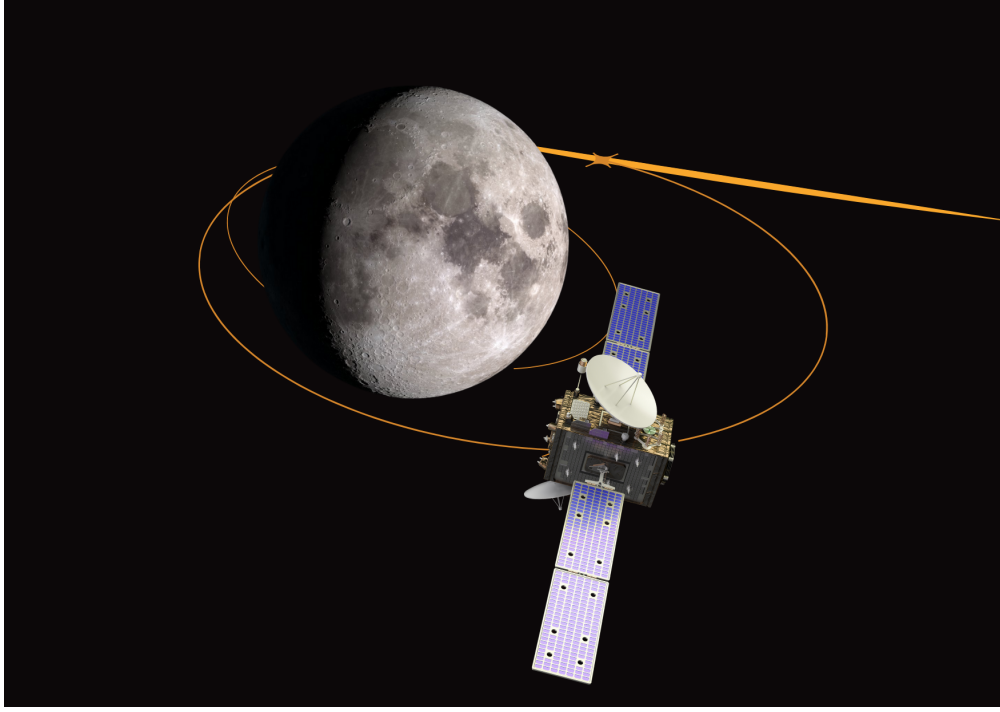


Figure 2: Conceptual Diagram of Lunar Orbit

- $r = \text{radius of Moon} + \text{orbital altitude} \approx 1737 \text{ km} + 200 \text{ km} = 1937 \text{ km}$
- $G = 6.674 \times 10^{-11} \text{ N}\cdot\text{m}^2/\text{kg}^2$
- $M = 7.342 \times 10^{22} \text{ kg}$ (Moon's mass)

Solving, the orbital period is ~ 1.9 hours, allowing about **12–13 orbits per Earth day**, which provides ample coverage opportunities over the mid-latitude region for descent planning and support.

2.2 Mission Phases

This mission is inspired by the architecture and sequence of the Chang'e 5 lunar sample return mission, but with key modifications to suit a new scientific goal—*the investigation of solar wind-derived water and plasma interactions in the Moon's mid-latitude region*, particularly around Oceanus Procellarum ($\sim 43^\circ\text{N}$). To achieve this, a carefully planned sequence of flight and surface phases is required, integrating established mission practices with customized adjustments for location, mission duration, and science payload.

2.2.1 Phase 1: Earth Launch

Similar to Chang'e 5, the mission begins with the launch of a multi-module spacecraft stack comprising the orbiter, lander, ascent vehicle, and Earth return capsule. A heavy-lift launch vehicle (e.g., Long March 5 or equivalent) places the stack into a low Earth orbit (LEO). The required delta-v for LEO insertion is typically about 9.3–10 km/s, including atmospheric drag and gravity losses:

$$\Delta v_{\text{LEO}} \approx 9.3 \text{ to } 10 \text{ km/s}$$

2.2.2 Phase 2: Trans-Lunar Injection (TLI)

A translunar injection burn propels the stack onto a lunar transfer trajectory. The ideal transfer uses a Hohmann-like elliptical trajectory from Earth orbit to the Moon's vicinity. The required delta-v is approximately 3.2 km/s from LEO:

$$\Delta v_{\text{TLI}} \approx 3.2 \text{ km/s}$$

2.2.3 Phase 3: Lunar Orbit Insertion (LOI)

On approaching the Moon, a retrograde burn decelerates the spacecraft and captures it into lunar orbit. Chang'e 5 used a ~ 200 km circular orbit with a 43° inclination to target Mons Rümker. For this mission, the target is still at $\sim 43^\circ$ N, but flexibility is allowed between 20° and 60° latitude, so the orbital inclination is adjusted accordingly:

$$\text{Orbital inclination } i \geq |\phi_{\text{target}}| \Rightarrow i \geq 43^\circ$$

2.2.4 Phase 4: Descent Maneuver and Surface Landing

The lander separates from the orbiter and begins a powered descent, including de-orbit burn, hazard avoidance, and soft touchdown near Oceanus Procellarum. Autonomous terrain-relative navigation (TRN), also used on Chang'e 3 and NASA's Mars 2020 missions, ensures accurate landing in mid-latitude terrain.

2.2.5 Phase 5: Lunar Surface Operations

A key difference from Chang'e 5 is the deployment of a mobile rover for extended science. The rover investigates volatile distribution, plasma interactions, and regolith composition. The mission duration is extended beyond Chang'e 5's 2-day surface operations to approximately 2–3 lunar days (56–84 Earth days), depending on thermal control and power systems.

2.2.6 Phase 6: Ascent and Phasing

After sampling, the ascent vehicle launches from the lander to enter lunar orbit. Phasing maneuvers align the ascent module with the orbiter. These use Hill's equations and patched-conic methods to optimize timing and energy.

$$\Delta v_{\text{rendezvous}} = \sqrt{\mu \left(\frac{2}{r} - \frac{1}{a} \right)} - V_{\text{orbit}}$$

2.2.7 Phases 7–9: Rendezvous and Docking (RVD)

Rendezvous operations are divided into far-range approach, close-range maneuvers, and autonomous docking. This mission adopts Chang'e 5's uncrewed RVD system, which uses visual and radar-based autonomous guidance.

2.2.8 Phase 10: Sample Transfer and Waiting

Once docked, the sample is transferred to the return capsule. The orbiter loiters in lunar orbit while waiting for optimal Earth alignment for return. This phase duration depends on orbital mechanics and mission timing.

2.2.9 Phase 11: Trans-Earth Injection (TEI)

A trans-Earth injection burn sends the return capsule toward Earth. The required delta-v for TEI is approximately 1.0 km/s.

2.2.10 Phase 12: Reentry and Recovery

The return capsule separates, enters Earth's atmosphere at ~ 11 km/s, and uses ablative heat shielding and parachutes for soft landing. Like Chang'e 5, the capsule is recovered from a predefined area (e.g., Inner Mongolia).

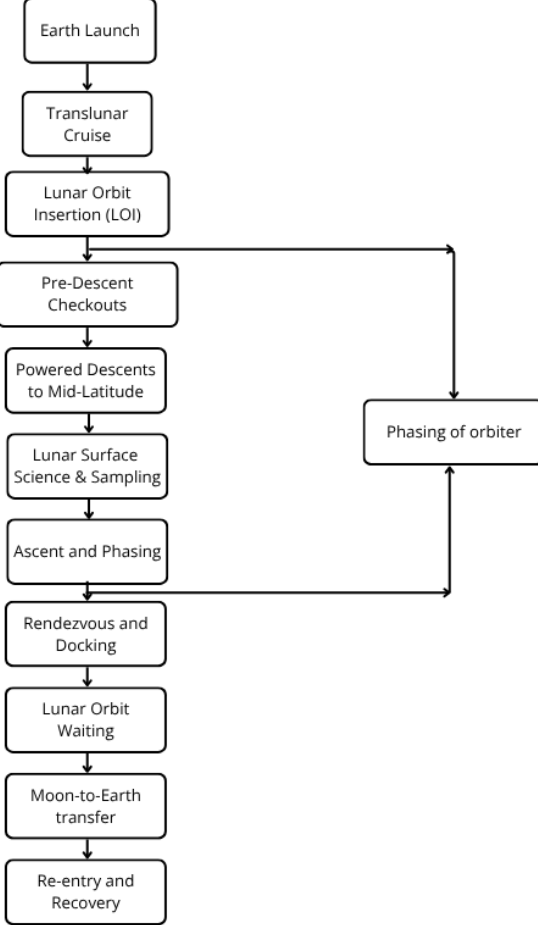


Figure 3: Flight Mission Profile

This flowchart outlines the complete flight profile for the lunar sample return mission targeting the mid-latitude region of the Moon, specifically around Oceanus Procellarum. The structure and sequence of phases in this mission are closely modeled after the successful Chang'e 5 mission, which demonstrated a highly efficient and autonomous lunar sample return architecture [14].

3 Technical Approach of Instruments, Subsystem, and Mission Operations

3.1 Spacecraft Overview

The spacecraft for this mission is a modular, multi-component system engineered to support a robotic sample return mission targeting the mid-latitude region of the Moon, particularly the *Oceanus Procellarum* (43°N). The spacecraft configuration draws inspiration from the successful *Chang'e 5* architecture, with significant

modifications to enable a longer-duration surface operation phase, incorporation of a mobile rover, and optimized sampling strategies for solar wind-derived volatiles.

The complete system is composed of five main modules. The **orbiter module** functions as the mission backbone during the Earth-Moon cruise, lunar orbiting, and final Earth return phases. It houses high-gain antennas and long-range communication systems for Earth-spacecraft data transmission, serves as the data relay between the lander/rover and mission control, supports rendezvous and docking operations after sample retrieval, and performs lunar orbit maintenance using onboard propulsion. The **lander module** is responsible for a soft landing at the designated mid-latitude site, delivering the rover and payload safely to the lunar surface. It serves as a temporary operations and charging hub for the rover, hosts some in-situ instruments such as the drill system and sample transfer arm, and supports the ascent module's launch. The **rover module** is a mobile platform designed to enhance this mission beyond Chang'e 5 by traversing geological sites within a 1–5 km radius. It conducts volatile profiling using instruments like the Ground Penetrating Radar (GPR), NIR/IR spectrometers, and regolith scoopers. The rover collects diversified regolith samples to constrain solar wind interaction and subsurface volatile distribution, operating autonomously over multiple lunar days (one lunar day \approx 14 Earth days) with solar-powered recharging. The **ascent vehicle** is mounted on the lander and is responsible for carrying the collected samples into lunar orbit. It initiates the rendezvous and docking sequence with the orbiter using autonomous launch and insertion, guided by proximity sensors and GPS-like systems. Compared to Chang'e 5, this version includes software enhancements and extended time windows to accommodate variable rover return schedules. Finally, the **return capsule** is ejected from the orbiter during the Earth return phase and reenters Earth's atmosphere with a heat shield, landing at a predesignated recovery site. It is engineered to preserve the scientific integrity of volatile-rich samples through advanced thermal and vacuum sealing technologies inspired by the OSIRIS-REx return capsule design.

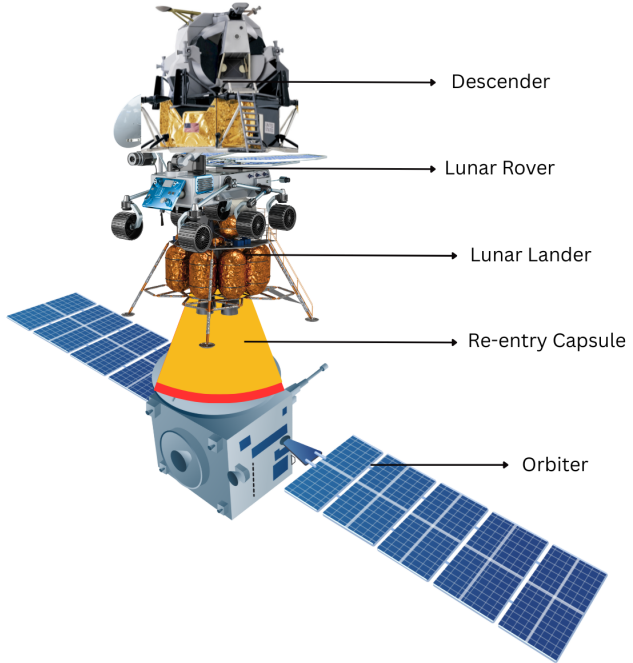


Figure 4: Conceptual layout showing key subsystems for the proposed lunar mission, including components adapted from previous missions such as Chang'e 5 (lander/ascent), Yutu-2 (rover), and OSIRIS-REx (return capsule).

3.2 Payload and Bus

The spacecraft for this mission is equipped with an advanced suite of scientific payloads and a robust spacecraft bus. The design is optimized for mid-latitude lunar sample return operations and in-situ analysis of solar wind-derived water. The payload is directly tied to the science objectives, while the bus ensures operational support throughout the mission lifecycle.

3.2.1 Payload Overview

The payload suite includes systems for sample acquisition, scientific measurement, and environmental monitoring. These instruments are specifically selected to maximize the scientific return from Oceanus Procellarum, a mid-latitude region identified for solar wind interactions [11, 6].

Sample Acquisition and Return System:

- Drill and Scooping Mechanism: A core sampling drill is designed to extract regolith from depths of up to 2 m. Previous findings [11] suggest that hydrogen implantation due to solar wind occurs within the top 1 meter of regolith, with deeper layers preserving historical implantation records.
- Sample Transfer Arm: Robotic arms guide regolith into sealed sample return canisters, ensuring minimal volatile loss.
- Vacuum-Sealed Canisters: Maintain lunar-like pressure and temperature to preserve volatiles, modeled by:

$$Q = mc\Delta T, \quad (1)$$

where Q is the thermal energy required to raise sample temperature, m is the mass of regolith, c is the specific heat ($\approx 700 \text{ J/kg} \cdot \text{K}$), and ΔT is the change in temperature. By maintaining $\Delta T \approx 0$, energy transfer is minimized.

Scientific Instruments:

- Near-Infrared Spectrometer (NIR): Measures absorption bands near $3 \mu\text{m}$ to detect OH/H₂O features. Modeled using Lambert-Beer law:

$$A = \log \left(\frac{I_0}{I} \right) = \epsilon cl, \quad (2)$$

where A is absorbance, I_0 and I are incident and transmitted light intensities, ϵ is molar absorptivity, c is concentration, and l is path length.

- Ground Penetrating Radar (GPR): Operates at dual-frequency bands to reveal stratigraphy and potential volatile pockets.
- Alpha Particle X-ray Spectrometer (APXS): Quantifies elemental abundance, especially hydrogen and oxygen.
- Solar Wind Collector: A passive collector to capture solar wind ions for isotopic analysis upon Earth return.

Navigation and Environmental Monitoring:

- Panoramic Cameras: High-resolution mapping of terrain and geological context.
- Thermal Radiometer: Monitors surface temperature fluctuations, which correlate with hydrogen mobility.

3.3 Spacecraft Bus Overview

The spacecraft bus is designed to support a range of mission functions including payload operation, orbital maneuvers, lunar surface activities, and autonomous sample return. Drawing inspiration from the Chang'e-5 mission architecture [15], the subsystems are engineered to balance performance, autonomy, and resilience in the harsh lunar environment.

3.3.1 Power Subsystem

- Deployable Solar Arrays: High-efficiency GaAs solar panels generate an average of 200 W during lunar daytime. The energy budget is calculated over a 14-day lunar day:

$$E_{\text{gen}} = P_{\text{avg}} \cdot t_{\text{day}} = 200 \text{ W} \cdot 336 \text{ hr} = 67.2 \text{ kWh}$$

- Lithium-Ion Batteries: Designed to store up to 1 kWh to support critical functions during the lunar night, with considerations for idle mode consumption.

3.3.2 Thermal Control Subsystem

- Multi-Layer Insulation (MLI): Protects internal components by minimizing radiative heat exchange with the extreme lunar environment.
- Active Thermal Management: Electrically powered heaters and dedicated radiators maintain subsystem temperatures within -40°C to $+50^{\circ}\text{C}$, modeled using the Stefan-Boltzmann law:

$$Q = \epsilon \sigma A (T^4 - T_{\text{env}}^4)$$

where ϵ is emissivity and A is radiator surface area.

3.3.3 Communication Subsystem

- UHF Antennas: Used for short-range communication between the lander and rover, ensuring robust low-latency control.
- X-band High-Gain Antenna: Facilitates long-distance transmission to Earth via a direct-to-Earth (DTE) link or relayed via the orbiter. Expected uplink/downlink data rates are 256 kbps and 512 kbps, respectively.

3.3.4 Propulsion Subsystem

- Bipropellant Engines: Enable orbit insertion, descent, ascent, and sample return phases. Mission Δv requirements are derived using:

$$\Delta v = I_{\text{sp}} \cdot g_0 \cdot \ln \left(\frac{m_0}{m_f} \right)$$

with total Δv budgeted at approximately 2.6 km/s.

- Cold Gas Thrusters: Provide precise attitude control for fine maneuvers and safe docking operations.

3.3.5 Command and Data Handling (C&DH)

- Fault-Tolerant Computers: Employ redundant logic with onboard storage of up to 256 GB. Capable of executing autonomous routines for descent, sampling, and rendezvous and docking (RVD).
- Autonomous Sequencing: Supports time-tagged command execution and contingency responses, crucial for real-time navigation and surface tasks.

3.3.6 Attitude Determination and Control System (ADCS)

- Sensor Suite: Star trackers, gyroscopes, inertial measurement units (IMUs), and Sun sensors provide 3-axis attitude determination with accuracy of $\pm 0.05^\circ$.
- Actuators: Reaction wheels and cold gas jets provide attitude control, especially during high-precision tasks like lunar orbit rendezvous and landing.

3.4 Mission Operations

Operations begin with pre-launch preparations including spacecraft integration, environmental testing, and ground segment readiness. The mission will rely on a network of ground stations for communication and tracking, potentially incorporating international support for global coverage.

Launch is achieved using a heavy-lift launch vehicle, such as the Long March 5 or Falcon Heavy, placing the spacecraft into a low Earth parking orbit. This is followed by a trans-lunar injection (TLI) burn that places the spacecraft on a translunar trajectory. Upon arrival at the Moon, a lunar orbit insertion (LOI) maneuver is executed to capture the spacecraft into a stable orbit.

Once in lunar orbit, phasing maneuvers align the descent module with the target site. The lander then performs a powered descent, autonomously guided by terrain-relative navigation and radar altimetry. Surface operations begin upon landing, during which the rover collects samples using a robotic arm and drill system, similar to the Chang'e 5 configuration. The anticipated surface duration is 24–48 hours, allowing for extended data collection and environmental monitoring beyond the 19-hour window used by Chang'e 5.

Following sample acquisition, the ascent module launches from the surface and enters lunar orbit to rendezvous and dock with the orbiter, where the sample container is transferred to the return capsule.

The final phase involves the trans-Earth injection (TEI) maneuver, after which the return capsule separates and reenters Earth's atmosphere. The sample return capsule is recovered upon touchdown, marking the mission's completion.

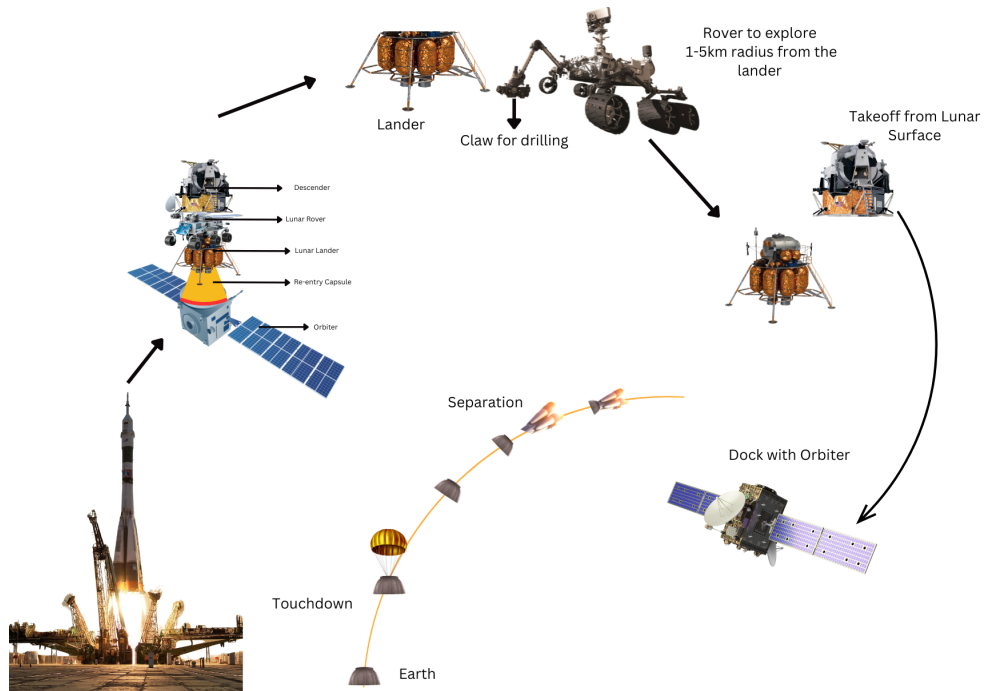


Figure 5: Conceptual Diagram of the Mission ConOps

3.5 Ground System and Data Dissemination

The system architecture includes Deep Space Network (DSN)-like ground stations with high-gain Earth antennas operating in the X-band or Ka-band frequencies, capable of tracking the lunar spacecraft and receiving high volumes of science and telemetry data. The Mission Control Center (MCC) is responsible for real-time command sequencing, spacecraft health monitoring, and the coordination of orbital maneuvers, lunar descent, and rover operations. Complementing this is the Science Operations Center (SOC), which manages the planning of science tasks, instrument scheduling, and scientific data review to ensure maximum return from payload instruments.

The Telemetry, Tracking, and Command (TT&C) infrastructure supports real-time telemetry reception from both the orbiter and lander, and two-way communication for command uplinks during all mission phases including orbit and surface operations. Tracking of the spacecraft is refined using Doppler measurements, ranging data, and delta-Differential One-way Ranging (delta-DOR) methods. For additional fault tolerance, a redundant low-gain antenna system is integrated to enable fail-safe backup communications.

Scientific and operational data will be transmitted in multiple phases. The initial transmission occurs during lunar orbit, where compressed science and health telemetry is relayed through orbiter passes. During the surface phase, data from the rover is relayed to the orbiter via UHF and subsequently downlinked to Earth in the X-band or Ka-band. After sample return, a final data dump will include sampling metadata, logs, and debrief reports. The dissemination process involves archiving both raw and processed data in a publicly accessible repository such as NASA's Planetary Data System (PDS) or CNSA's data repository. Early access to the dataset will be granted to mission collaborators and the science team, followed by broader release accompanying publications and international workshops.

To reduce latency and optimize bandwidth, the system incorporates onboard data compression and prioritization algorithms. Ground-based systems will utilize automated pipelines to sort, filter, and classify incoming telemetry. Moreover, artificial intelligence may assist in real-time or near-real-time identification of regions of interest from rover-acquired imagery, enabling adaptive science planning.

Assuming a data generation rate from rover-based imagery and spectrometry of approximately 10 GB/day, and an X-band downlink rate of 1 Mbps using a 35-meter Earth-based dish, the communication link can support substantial daily downlink capacity. With an available communication window of 6 hours per day, the data volume transmitted is calculated as:

$$\text{Daily Downlink Capacity} = 1 \text{ Mbps} \times 3600 \text{ s/hr} \times 6 \text{ hr} = 21.6 \text{ GB}$$

This provides a comfortable margin for daily science and telemetry transmission needs, enabling efficient and secure return of mission-critical information from lunar orbit and surface operations.

4 Space Environment Issues

As the spacecraft exits Low Earth Orbit and transitions toward the Moon, it encounters numerous environmental and operational hazards.

4.1 Identification of Threat Sources

One of the primary challenges involves thermal cycling due to the absence of atmospheric convection. All thermal regulation must rely solely on radiative mechanisms, and alternating exposure to direct solar flux leads to repeated heating and cooling of spacecraft surfaces. These temperature fluctuations induce thermal expansion and contraction, leading to material fatigue. The net radiative heat exchange from the spacecraft to space is governed by the Stefan–Boltzmann law:

$$Q = \epsilon\sigma A (T^4 - T_{\text{space}}^4)$$

where ϵ is the emissivity of the surface, σ is the Stefan–Boltzmann constant, A is the radiative area, T is the spacecraft's surface temperature, and T_{space} is the background temperature of deep space, typically approximated as 3 K.

Radiation exposure intensifies significantly during transit through the Van Allen belts. These zones, populated by energetic electrons and protons, pose severe risks to onboard electronics and sensors, especially in the form of total ionizing dose (TID) accumulation and bit errors. Another major concern is electrostatic charging and discharging events. In the sparse plasma regions of the outer magnetosphere, differential charging between spacecraft surfaces becomes likely, potentially culminating in electrostatic discharges (ESDs) that can damage avionics or interfere with signal integrity.

Solar Particle Events (SPEs), caused by solar flares and coronal mass ejections, are capable of delivering high-energy protons that penetrate spacecraft shielding. These particles may trigger single-event upsets (SEUs) or latch-ups in integrated circuits. Moreover, in the micrometeoroid environment of cis-lunar space, relative velocities can reach 20–70 km/s, making even sub-millimeter particles highly destructive. The kinetic energy associated with such impacts is given by:

$$E_k = \frac{1}{2}mv^2$$

where m is the mass of the micrometeoroid and v is its relative velocity with respect to the spacecraft.

During this orbital phase, the communication links can suffer from signal dropouts due to terrain-induced line-of-sight obstruction or complete occultation behind the lunar limb. Attitude drift during this phase may arise from minor micrometeoroid impacts or uneven mass distribution, which may alter the spacecraft's moment of inertia and torque balance.

During descent, the lunar surface—electrostatically charged by solar ultraviolet radiation and the solar wind—can eject dust particles that may strike the vehicle or charge ungrounded surfaces. These interactions may influence vehicle systems and compromise the cleanliness of sensitive components like the Alpha Particle X-ray Spectrometer, Solar Wind Collector and the likes.

One of the most persistent challenges in surface operations is the fine, abrasive nature of lunar regolith, which adheres to optics, thermal radiators, joints, and seals via electrostatic attraction and mechanical embedding. This dust can degrade optical clarity and reduce thermal control efficiency.

The lunar environment also imposes extreme temperature conditions, with daytime temperatures reaching up to +120°C and nighttime plunging to as low as –180°C. Moreover, in the absence of a significant magnetic field, the surface is directly exposed to galactic cosmic rays (GCRs) and sporadic solar particle events (SPEs), increasing radiation dosage to both humans and electronics.

Residual dust from surface activities poses a risk to critical components such as pyrovalves, mechanical latches, and nozzle apertures, potentially impairing separation events or degrading engine performance. Thermal instability is especially problematic during nighttime launches, where structural elements may have undergone significant contraction. Additionally, charging effects in lunar orbit can generate differential potentials between separate vehicle elements, influencing signal grounding or avionics behavior. Optical sensors used for rendezvous or navigation may be affected by sun glint or reflected lunar albedo, introducing further complexity into visual tracking and imaging tasks.

4.2 Threat Assessment

As of June 2, 2025, the Sun is exhibiting elevated activity characteristic of the solar maximum phase of Solar Cycle 25, which is expected to peak around July 2025 [16]. Notably, an M8.2-class solar flare was observed on May 31, 2025, originating from active region AR4100 [17]. This triggered a G4 (Severe) geomagnetic storm that impacted Earth on June 1 [18], producing auroras seen across North America and as far south as New South Wales, Australia [19]. NOAA's Space Weather Prediction Center (SWPC) has maintained a G4 storm watch into June 2, indicating a sustained period of intense geomagnetic activity [18]. Given the scheduled lunar launch in October 2026—during the peak of solar activity—this increased solar environment presents notable risks for spacecraft design and mission planning.

Given the planned lunar mission launch in October 2026, during the peak of solar activity, it's crucial to assess potential space weather threats. The table below summarizes key solar-related threats, their likelihood, potential impact, and the necessity for mitigation:

Threat Source	Encounter Likelihood	Danger Level if Encountered	Mitigation Need
Solar Particle Events (SPEs)	High	High	Absolutely Yes
Coronal Mass Ejections (CMEs)	Moderate to High	High	Absolutely Yes
Solar Flares (X-class)	Moderate	Moderate to High	Strongly Recommended
Geomagnetic Storms (G3–G4)	High	Moderate	Strongly Recommended
Increased Solar UV Radiation	High	Low to Moderate	Necessary
Radio Blackouts (HF/VHF)	Moderate	Moderate	Necessary
Satellite Charging Events	High	High	Absolutely Yes
GPS Signal Degradation	Moderate	Moderate	Necessary
Thermal Variability from Solar Flux	High	Moderate	Strongly Recommended

Table 1: Although the space environment is inherently uncertain and it is impractical to design a spacecraft that is completely immune to all hazards, the color-coded assessment in the table provides a structured evaluation of solar activity-related threats for the October 2026 lunar mission. Red highlights indicate high-priority risks that demand immediate mitigation. Orange signifies moderate to high risks requiring proactive planning. Green represents lower-priority risks, which may be tolerable but should not be ignored without careful consideration.

4.3 Components at Risk and Failure Mechanisms Due to Solar Activity

The space environment during the proposed October 2026 lunar mission is expected to be particularly harsh due to the peak of Solar Cycle 25. Several spacecraft subsystems are vulnerable to heightened solar activity and associated phenomena such as Solar Particle Events (SPEs), Coronal Mass Ejections (CMEs), geomagnetic storms, and enhanced ultraviolet and X-ray radiation. These space weather events pose distinct risks to spacecraft components, each with specific failure mechanisms.

Avionics and Onboard Electronics: High-energy protons from SPEs and electrons from radiation belts can penetrate shielding and cause Single Event Upsets (SEUs), latch-ups, or even permanent damage to microelectronic components. CMOS-based processors are particularly vulnerable. Charge accumulation due to differential charging can lead to electrostatic discharge (ESD), damaging circuits and inducing transient faults.

Power Systems (Solar Arrays and Batteries): Increased solar flux from flares or CMEs can temporarily boost solar panel output, but long-term exposure degrades photovoltaic efficiency. SPE-induced ionizing radiation can also damage battery chemistry, reducing charge capacity and altering discharge profiles.

Communication Systems: High-frequency (HF) and very high-frequency (VHF) radio signals may be attenuated or lost during solar radio bursts or when passing through regions affected by ionospheric disturbances. CMEs and flares can cause signal blackouts, particularly during critical mission phases such as descent or ascent.

Thermal Control Subsystems: Fluctuations in solar irradiance during active solar periods introduce thermal instability. The spacecraft is subjected to extreme temperature cycling, resulting in thermal stress and fatigue in radiators, coatings, and surface-mounted sensors. This can degrade material properties over time and compromise radiator performance.

Attitude Determination and Control System (ADCS): Increased solar albedo and glint may saturate star trackers or sun sensors, reducing pointing accuracy. Additionally, momentum buildup due to differential radiation pressure or magnetic torque during geomagnetic storms can disrupt attitude stability.

Structure and Mechanisms: Charging from the lunar surface environment and solar wind interaction can affect separation mechanisms, such as pyrotechnics or release actuators. Residual dust from electrostatic

levitation may settle on moving parts, increasing friction or impairing deployment of antennas or instruments.

Navigation Systems: Solar activity can introduce errors in GPS signals and degrade navigation accuracy. In deep space, where GPS coverage is absent, optical navigation and inertial systems may be disrupted by sun glint, albedo variation, or instrument drift under thermal gradients.

These effects are amplified during active solar periods and necessitate robust fault tolerance and radiation-hardened design to ensure mission success.

4.4 Risk Management and Mitigation Strategies

In light of the identified threats from heightened solar activity, a comprehensive risk management plan is essential to enhance spacecraft survivability and ensure mission continuity. Radiation-hardened design must be prioritized, with all critical avionics and command systems employing radiation-hardened microprocessors and memory units. Triple Modular Redundancy (TMR), Error Detection and Correction (EDAC) coding, and watchdog timers should be integrated to recover from Single Event Upsets or bit flips. Shielding strategies, particularly with materials like polyethylene, will attenuate high-energy protons and electrons; critical components should be located deeper within the spacecraft to maximize shielding. Thermal and electrical isolation must be ensured via thermal coatings, active radiators, and robust grounding to minimize differential charging, while surge suppressors and ESD protection devices should protect sensitive circuits. Real-time space weather monitoring through platforms such as NOAA's DSCOVR or NASA's ACE will allow safe-mode protocols to be activated during solar events, including spacecraft reorientation or operational pauses. Autonomous fault detection and recovery via rules-based logic or machine learning systems will enhance response during communication delays by isolating faults and ensuring graceful subsystem degradation. Redundant communication pathways using dual-band channels (e.g., S-band and X-band) and relay support via lunar orbiters will reduce the risk of blackouts, and dynamic bandwidth allocation with error correction will sustain data flow. Mission timeline optimization should avoid periods of expected solar maxima or geomagnetic storm forecasts and include contingencies such as loitering or delayed descent plans. Dust mitigation techniques such as magnetic deflectors, electrodynamic screens, and recessed optics should be integrated into lander and rover systems to prevent contamination or mechanical failure. Post-launch risk review routines must include regular health checks and integration of current space weather forecasts, using risk matrices or decision trees to support go/no-go decision-making. Implementing these layered defenses will not eliminate all risks, but they substantially enhance spacecraft resilience during the solar maximum conditions anticipated in October 2026.

5 Conclusion

As humanity continues to push the boundaries of space exploration, missions to the Moon and beyond must contend with an increasingly dynamic and hostile space environment—none more pressing than the threats posed by heightened solar activity. The projected October 2026 lunar mission will coincide with the peak of Solar Cycle 25, introducing amplified risks from solar particle events, geomagnetic storms, and electrostatic disturbances. Through detailed analysis, we have identified critical spacecraft components most vulnerable to solar-induced failures and developed a multi-layered mitigation strategy encompassing engineering design, operational protocol, and real-time risk management.

From radiation-hardened avionics and shielding architectures to autonomous fault recovery systems and mission timeline optimization, our integrated risk management framework underscores the importance of proactive planning in mission assurance. While no system is impervious to the unpredictable nature of space weather, adopting these strategies significantly enhances spacecraft resilience, operational reliability, and crew safety. This project not only provides a robust threat-response model tailored for lunar operations but also contributes to a growing body of best practices applicable to deep space missions during solar maxima. As we prepare to return to the Moon under the glow of a volatile Sun, the rigor and foresight demonstrated in this assessment stand as both a technological safeguard and a testament to the ingenuity of modern aerospace engineering.

References

- [1] Croots, A. P. S., "Water on The Moon, I. Historical Overview," *Astronomical Review*, Vol. 6, No. 7, 2011, pp. 4–20, Available at: <https://doi.org/10.1080/21672857.2011.11519687>.
- [2] Chen, X., Yang, S., Chen, G., Xu, W., Song, L., Li, A., Yin, H., Xia, W., Gao, M., Li, M., Wu, H., Cui, J., Zhang, L., Miao, L., Shui, X., Xie, W., Ke, P., Huang, Y., Sun, J., Yao, B., and Bai, H., "Massive water production from lunar ilmenite through reaction with endogenous hydrogen," *The Innovation*, Vol. 5, No. 6, 2024, pp. 100690, Available at: <https://doi.org/10.1016/j.xinn.2024.100690>.
- [3] Pieters, C. M., Goswami, J., Clark, R., et al., "Character and spatial distribution of OH/H₂O on the surface of the Moon seen by M3 on Chandrayaan-1," *Science*, Vol. 326, No. 5952, 2009, pp. 568–572, Available at: <https://doi.org/10.1126/science.1178658>.
- [4] Colaprete, A., Schultz, P. H., et al., "Detection of water in the LCROSS ejecta plume," *Science*, Vol. 330, No. 6003, 2010, pp. 463–468, Available at: <https://doi.org/10.1126/science.1186986>.
- [5] Anand, M., "Lunar Water: A Brief Review," *Earth, Moon, and Planets*, Vol. 107, No. 1, 2010, pp. 65–73, Available at: <https://doi.org/10.1007/s11038-010-9377-9>.
- [6] Zhou, C., Tang, H., Li, X., Zeng, X., Mo, B., Yu, W., Wu, Y., Zeng, X., Liu, J., and Wen, Y., "Chang'E-5 samples reveal high water content in lunar minerals," *Nature Communications*, Vol. 13, 2022, pp. 5601, Available at: <https://doi.org/10.1038/s41467-022-33095-1>.
- [7] Wang, H. Z., Zhang, J., Shi, Q. Q., Saito, Y., Degeling, A. W., Rae, I. J., Liu, J., Guo, R. L., Yao, Z. H., Tian, A. M., Fu, X. H., Zong, Q. G., Liu, J. Z., Ling, Z. C., Sun, W. J., Bai, S. C., Chen, J., Yao, S. T., Zhang, H., Wei, Y., Liu, W. L., Xia, L. D., Chen, Y., Feng, Y. Y., Fu, S. Y., and Pu, Z. Y., "Earth wind as a possible source of lunar surface hydration," *Nature Astronomy*, 2023, Available at: <https://doi.org/10.48550/arXiv.1903.04095>.
- [8] Burke, D., Koziar, J., Liu, Y., Ichimura, A., Dyar, M. D., Lane, M. D., and Taylor, L. A., "NASA experimental evidence for solar wind-induced hydroxylation of lunar regolith," *Lunar and Planetary Science Conference*, Vol. 42, 2011, pp. 2392, Available at: <https://doi.org/10.5194/egusphere-egu23-9917>.
- [9] Szymanski, A., Schaible, M., Baragiola, R. A., and Orlando, T. M., "Laboratory simulations of water formation via solar wind interactions with silicate grains," *Journal of Geophysical Research: Planets*, Vol. 124, No. 3, 2019, pp. 568–577, Available at: <https://doi.org/10.1029/2018JE005765>.
- [10] Li, S., Lucey, P. G., Milliken, R. E., Hayne, P. O., Fisher, E., Williams, J.-P., Hurley, D. M., and Elphic, R. C., "Direct evidence of surface exposed water ice in the lunar polar regions," *Proceedings of the National Academy of Sciences*, Vol. 115, No. 36, 2020, pp. 8907–8912, Available at: <https://doi.org/10.1073/pnas.1802345115>.
- [11] Li, Y., Sun, Y., Liu, D., et al., "High abundance of solar wind-derived water in lunar soils from the middle latitude," *Nature Communications*, Vol. 14, No. 1, 2023, pp. 2452, Available at: <https://doi.org/10.1073/pnas.2214395119>.
- [12] Qian, W. et al., "The engineering and realization of the Chinese Lunar Exploration Project," *Journal of Geophysical Research: Planets*, Vol. 123, No. 6, 2018, pp. 1328–1340, Available at: <https://doi.org/10.1029/2018JE005595>.
- [13] Administration, C. N. S., "Chang'e-5 Lunar Sample Return Mission Summary," 2020, <https://www.cnsa.gov.cn/english/n6465652/n6465653/c6810692/content.html>.
- [14] Wang, Z.-S., Meng, Z., Gao, S., and Peng, J., "Orbit Design Elements of Chang'e 5 Mission," *Space: Science & Technology*, 2021, Available at: <https://doi.org/10.34133/2021/9897105>.
- [15] ESA EO Portal, "Chang'e-5 Mission," <https://www.eoportal.org/satellite-missions/chang-e-5>, 2021, Accessed: 2025-05-26.

- [16] NOAA Space Weather Prediction Center, “Solar Cycle Progression,” <https://www.swpc.noaa.gov/products/solar-cycle-progression>, 2025, Accessed: 2025-06-02.
- [17] País, E., “La Agencia Espacial Española lanza advertencia tras intensa eyeción solar,” <https://elpais.com/ciencia/2025-06-02/la-agencia-espacial-espanola-lanza-advertencia-tras-intensa-eyecion-solar.html>, 2025, Accessed: 2025-06-02.
- [18] NOAA SWPC, “G4 (Severe) Geomagnetic Storm Watch in Effect for 2 June,” <https://www.swpc.noaa.gov/news/g4-severe-geomagnetic-storm-watch-effect-2-june-utc-day>, 2025, Accessed: 2025-06-02.
- [19] India, E. T., “Northern Lights in US: These 13 States to Witness Aurora Today,” <https://economictimes.indiatimes.com/news/international/global-trends/northern-lights-in-us-these-13-states-to-witness-aurora-today-heres-how-you-can-maximize-your-view/articleshow/121569805.cms>, 2025, Accessed: 2025-06-02.